Hydrothermal Synthesis and Characterization of Two New Zinc Phosphates Assembled about a Chiral Metal Complex: $[Co^{II}(en)_3]_2[Zn_6P_8O_{32}H_8]$ and $[Co^{III}(en)_3][Zn_8P_6O_{24}Cl]\cdot 2H_2O$

Jihong Yu, Yu Wang, Zhan Shi, and Ruren Xu*

State Key Laboratory of Inorganic Synthesis and Preparative Chemistry, Jilin University, Changchun 130023, People's Republic of China

Received April 3, 2001. Revised Manuscript Received July 10, 2001

A racemic mixture of the chiral metal complex $Co(en)_3Cl_3$ has been used in the hydrothermal synthesis of the layered compound $[Co^{II}(en)_3]_2[Zn_6P_8O_{32}H_8]$ (**1**) and the three-dimensional connected framework compound $[Co^{III}(en)_3][Zn_8P_6O_{24}Cl]\cdot 2H_2O$ (**2**). Their structures were determined by single-crystal X-ray diffraction analyses and further characterized by X-ray powder diffraction, ICP, elemental, and TG analyses. The structure of **1** consists of vertex-linking ZnO_4 and $PO_3(OH)$ tetrahedral units forming macroanionic sheets with 4.6.8 nets. The framework structure of **2** built up of ZnO_4, ZnO_3Cl, and PO_4 tetrahedra can be viewed as stacking of the zinc phosphate layers along the *c* axis linked by Cl atoms as pillars to generate intersecting tunnels with 12-membered-ring windows. Both structures **1** and **2** contain chiral structural motifs, the chiral characters of which are believed to be transferred from the chiral metal complex. The enantiomers of $Co(en)_3Cl_3$ are separated as Δ and Λ configurations in the structures of both **1** and **2** and interact with the inorganic hosts through H-bonding interactions. Crystal data: **1**, monoclinic, *C*2/*c*, $a = 16.623(2)$ Å, $b = 30.589(5)$ Å, $c = 17.441(2)$ Å, $\beta = 90.35(1)°$, $Z = 8$; **2**, trigonal, *P*-31*c*, $a = 8.8775(7)$ Å, $c = 23.775(3)$ Å, $Z = 2$.

Introduction

Chiral nanoporous materials are especially desirable for enantioselective separation and catalysis, which are important in the chemical and pharmaceutical industries.[1,2] To date, porous materials created by templates have been largely achiral. Only a small number of chiral metal phosphates have been prepared using achiral templates. Several such compounds are $[NH_3(CH_2)\text{-}NH_2(CH_2)_2NH_3][(ZnPO_4)(HPO_4)]$,[3] $[CN_3H_6][Sn_4P_3O_{12}]$,[4] $[(CH_3)NH_2]K_4[V_{10}O_{10}(H_2O)_2(OH)_4(PO_4)_7]4H_2O$,[5] ULM-5,[6] and UCSB-7.[7] The control of chirality is particularly difficult because of the unclear mechanism by which the inorganic framework is assembled by the template.

Recently, the employment of a chiral metal complex as a templating agent by Morgan[8] and by Wilkinson et al.[9−11] has opened up the possibility for the design of nanoporous materials with chirality. Notable examples are the syntheses of a couple of two-dimensional layered aluminophosphate compounds using an optically pure chiral metal complex or a racemic mix of chiral metal complex as the template.[8−11] It appears that the chirality of the metal complex can be transferred to the inorganic networks through the formation of the "chiral pockets" in $[Co(en)_3][Al_3P_4O_{16}]3H_2O$[8] and the chiral sheet in $[d\text{-}Co(en)_3][Al_3P_4O_{16}]3H_2O$.[11] On the other hand, interestingly, in Gtex2, $[Co(tn)_3][Al_3P_4O_{16}]2H_2O$,[9] there exists a spontaneous enantiomeric separation when this compound is synthesized using a racemic mixture of $[Co(tn)_3]^{3+}$ as a template.

A fascinating subject thus aroused is the transference of chirality from the metal complex to the inorganic host and the molecular recognition ability of the inorganic host for the guest chiral metal complex. In this work, a racemic mixture of the chiral metal complex $Co(en)_3Cl_3$ has been used in the synthesis of a zinc phosphate system. Among metal phosphates, zinc phosphates templated by organic amines show very rich structural and compositional diversity with one-dimensional (1D) chain, 2D layer, and 3D open-framework structures.[12−22] Herein, the preparation and analysis of two $Co(en)_3Cl_3$-

(1) Baiker, A. *Curr. Opin. Solid State Mater. Sci.* **1996**, *3*, 86.
(2) Davis, M. E. *Acc. Chem. Res.* **1993**, *26*, 111.
(3) Neeraj, S.; Natarajan, S.; Rao, C. N. R. *Chem. Commun.* **1999**, 165.
(4) Ayyappan, S.; Bu, X.; Cheetham, A. K.; Rao, C. N. R. *Chem. Mater.* **1998**, *10*, 3308.
(5) Sghomonian, V.; Chen, Q.; Haushalter, R. C.; Zubieta, J.; O'Connor, C. J. *Science* **1993**, *259*, 1596.
(6) Francis, R. J.; O'Brien, S.; Fogg, A. M.; Halasyamani, P. S.; Loiseau, D. T.; Férey, G. *J. Am. Chem. Soc.* **1999**, *121*, 1002.
(7) Gier, T. E.; Bu, X.; Feng, P.; Stucky, G. D. *Nature* **1998**, *395*, 154.
(8) Morgan, K.; Gainsford, G.; Milestone, N. *J. Chem. Soc., Chem. Commun.* **1995**, 425.
(9) Bruce, D. A.; Wilkinson, A. P.; White, M. G.; Bertrand, J. A. *J. Chem. Soc., Chem. Commun.* **1995**, 2059.
(10) Bruce, D. A.; Wilkinson, A. P.; White, M. G.; Bertrand, J. A. *J. Solid State Chem.* **1996**, *125*, 228.
(11) Gray, M. J.; Jasper, J. D.; Wilkinson, A. P. *Chem. Mater.* **1997**, *9*, 976.
(12) Harrison, W. T. A.; Gier, T. E.; Moran, K. L.; Eckert, H.; Stucky, G. D. *Chem. Mater.* **1991**, *3*, 27.
(13) Nenoff, T. M.; Harrison, W. T. A.; Gier, T. E.; Stucky, G. D. *J. Am. Chem. Soc.* **1991**, *113*, 378.
(14) Harrison, W. T. A.; Nenoff, T. M.; Gier, T. E.; Stucky, G. D. *Inorg. Chem.* **1992**, *31*, 5395.

10.1021/cm010302f CCC: $20.00
Published on Web 09/17/2001

Table 1. Crystal Data and Structure Refinement for Compounds 1 and 2

	1	**2**
formula	$C_{12}H_{56}Co_2N_{12}O_{32}P_8Zn_6$	$C_6H_{28}ClCoN_6O_{26}P_6Zn8$
fw	1638.53	1404.50
space group	*C*2/*c*	$P\bar{3}1c$
a, Å	16.623(2)	8.8775(7)
b, Å	30.589(5)	8.8775(7)
c, Å	17.441(2)	23.775(3)
$\beta(\gamma)$, degrees	90.352(10)	120
volume, Å^3	8868(2)	1622.7(2)
Z	8	2
refltn collected/unique	36116/12601 [*R*(int) = 0.0982]	6159/793 [*R*(int) = 0.1194]
D_{calcd}, g cm^{-3}	2.454	2.872
μ, mm^{-1}	4.322	6.788
temp (K)	293(2)	293(2)
F(000)	6576	1376
θ range for data collection, degrees	1.33−30.02	1.71−23.34
limiting indices	$-17 \le h \le 23$, $-41 \le k \le 39$, $-24 \le l \le 23$	$-6 \le h \le 9$, $-9 \le k \le 5$, $-25 \le l \le 26$
refinement method	full-matrix least-squares on F^2	full-matrix least-squares on F^2
data/restraints/parameters	12601/0/650	793/0/84
goodness-of-fit on F^2	0.899	1.162
final *R* indices [$I > 2\sigma(I)$]	$R_1 = 0.0515$, $wR_2 = 0.0893$	$R_1 = 0.0410$, $wR_2 = 0.1078$
R indices (all data)	$R_1 = 0.1572$, $wR_2 = 0.1101$	$R_1 = 0.0423$, $wR_2 = 0.1089$
largest diff peak and hole, e Å^{-3}	1.313 and −0.790	0.780 and −0.910

templated zinc phosphates, [Co^{II}(en)$_3$]$_2$[Zn$_6$P$_8$O$_{32}$H$_8$] (**1**) and [Co^{III}(en)$_3$][Zn$_8$P$_6$O$_{24}$Cl]·2H$_2$O (**2**), with novel structural architectures is described. This work provides a clear example of how recognition phenomena between a chiral metal complex guest and an inorganic host framework can lead to the crystallization of structures that retain the chiral character of the guest.

Experimental Section

Synthesis. Compounds **1** and **2** were synthesized through the hydrothermal reaction of a mixture of Zn(OAc)$_2$, H$_3$PO$_4$, Co(en)$_3$Cl$_3$, and H$_2$O in a molar ratio of 1.0:2.0:0.25:122. Typically, 1 g of Zn(OAc)$_2$ was first dissolved in 10 mL of H$_2$O, and then 0.44 g Co(en)$_3$Cl$_3$ was added with stirring. Finally, 0.62 mL of H$_3$PO$_4$ (85 wt %) was added dropwise to the above reaction mixture. A gel was formed and stirred for an additional 1 h until it was homogeneous; then, it was sealed in a Teflon-lined stainless steel autoclave and heated at 145 °C for 26 h under static conditions. The filling volume of the reaction gel in the autoclave was critical for the final product. The products were separated by sonication, further washed by distilled water, and then air-dried.

Characterization. X-ray powder diffraction (XRD) data were collected on a Siemens D5005 diffractometer with Cu Kα radiation (λ = 1.5418 Å). The elemental analyses were conducted on a Perkin-Elmer 2400 elemental analyzer. Inductively coupled plasma (ICP) analysis was performed on a Perkin-Elmer Optima 3300DV spectrometer. Energy-dispersive X-ray analysis was performed on a JEM 2000FK electron microscope. A Perkin-Elmer TGA 7 unit was used to carry out the thermogravimetric analysis (TGA) in air at a heating rate of 20 °C/min.

Structural Determination. Suitable single crystals with dimensions of 0.6 × 0.08 × 0.08 mm for **1** and 0.8 × 0.4 × 0.1 mm for **2** were selected for single-crystal X-ray diffraction analysis. Structural analysis was performed on a Siemens SMART CCD diffractometer using graphite-monochromated Mo Kα radiation (λ = 0.71073 Å). The data were collected at a temperature of 20 ± 2 °C. Data processing was accomplished with the SAINT processing program.[23] Direct methods were used to solve the structure using the SHELXL crystallographic software package.[24] All non-hydrogen atoms were easily found from the difference Fourier map. For compound **2**, the existence of Cl atoms was suggested by the energy-dispersive X-ray analysis, as well as the suitable thermal parameters. H atoms attached to the terminal P−O group in **1** and to the metal complex in **1** and **2** were placed geometrically and refined using a riding model. Hydrogen atoms on the water molecules in **2** were not located because of the large thermal parameter of O$_w$. All non-hydrogen atoms were refined anisotropically. Experimental details for the structural determinations of **1** and **2** are presented in Table 1. The final atomic coordinates for **1** and **2** are presented in Tables 2 and 3, respectively.

Results and Discussion

Both compounds **1** and **2** are synthesized in a gel with a molar composition 1.0 Zn(OAc)$_2$:2.0 H$_3$PO$_4$:0.25 Co(en)$_3$Cl$_3$:122 H$_2$O in a temperature range of 140−150 °C. At first, we found that it was very difficult to reproduce the product. On careful examination of the influencing factors, it was noticed that the filling volume is a critical factor affecting the formation of **1** and **2**. If the filling volume is 50%, large single crystals of **1** are obtained. If the filling volume is above 80%, large single crystals of **2** are obtained. When the filling volume is between 50% and 80%, **1** and **2** coexist in the product. As the filling volume increases, **2** dominates in the product. It is noted that a small amount of zinc phosphate, Zn$_6$(PO$_4$)$_4$(HPO$_4$)(H$_2$O)(H$_3$NCH$_2$CH$_2$NH$_3$),[19] is always formed in the product, the template molecule H$_2$NCH$_2$CH$_2$NH$_2$ of which is produced by the partial decomposition of the cobalt complex. That the filling volume affects the products to such a great extent indicates that the pressure of the reaction system has a tremendous influence on the product under above hydrothermal conditions. To further validate this observation, we used a solvent

(15) Harrison, W. T. A.; Nenoff, T. M.; Gier, T. E.; Stucky, G. D. *Inorg. Chem.* **1993**, *32*, 2437.
(16) Song, T.; Hurshouse, M. B.; Chen. J.; Xu, J.; Malik, K. M. A.; Jones, R. H.; Xu, R.; Thomas, J. M. *Adv. Mater.* **1994**, *6*, 679.
(17) Harrison, W. T. A.; Dussak L. L.; Jacobson, A. J. *J. Solid State Chem.* **1996**, *125*, 134.
(18) Harrison, W. T. A.; Bircsak, Z.; Hannoman, L.; Zhang, Z. *J. Solid State Chem.* **1998**, *136*, 93.
(19) Harmon, S. B.; Sevov, S. C. *Chem. Mater.* **1998**, *10*, 3020.
(20) Neeraj, S.; Natarajan, S.; Rao, C. N. R. *Chem. Mater.* **1999**, *11*, 1390.
(21) Yang, G. Y.; Sevov, S. C. *J. Am. Chem. Soc.* **1999**, *121*, 8389.
(22) Neeraj, S.; Natarajan, S. *Chem. Mater.* **2000**, *12*, 2753.
(23) SMART and SAINT software packages; Siemens Analytical X-ray Instruments, Inc.: Madison, WI, 1996.
(24) Sheldrick, G. M. *SHELXL Program*, version 5.1; Siemens Industrial Automation, Inc.: Madison, WI, 1997.

Table 2. Atomic Coordinates ($\times 10^4$) and Equivalent Isotropic Displacement Parameters ($Å^2 \times 10^3$) for 1

	x	*y*	*z*	*U*(eq)[a]
Co(1)	7532(1)	1573(1)	2491(1)	16(1)
Co(2)	5000	914(1)	7500	17(1)
Co(3)	0	937(1)	7500	14(1)
Zn(1)	−1304(1)	2467(1)	5337(1)	21(1)
Zn(2)	560(1)	1738(1)	4974(1)	18(1)
Zn(3)	1239(1)	−45(1)	5248(1)	18(1)
Zn(4)	4012(1)	1916(1)	5298(1)	18(1)
Zn(5)	3499(1)	575(1)	4633(1)	21(1)
Zn(6)	6940(1)	771(1)	5098(1)	21(1)
P(1)	−2460(1)	3241(1)	4829(1)	21(1)
P(2)	325(1)	2553(1)	6153(1)	17(1)
P(3)	−176(1)	2431(1)	3820(1)	17(1)
P(4)	50(1)	742(1)	4830(1)	17(1)
P(5)	2368(1)	1406(1)	5175(1)	18(1)
P(6)	5130(1)	1087(1)	4830(1)	19(1)
P(7)	7142(1)	−37(1)	3946(1)	16(1)
P(8)	7670(1)	70(1)	6277(1)	16(1)
O(1)	−2163(3)	2915(2)	5429(2)	21(1)
O(2)	−528(3)	2748(2)	6031(3)	25(1)
O(3)	−892(3)	2567(2)	4319(3)	32(1)
O(4)	−1777(3)	1914(2)	5552(3)	34(1)
O(5)	320(3)	2073(2)	5894(3)	27(1)
O(6)	127(3)	1984(2)	4046(3)	34(1)
O(7)	5(3)	1187(2)	5195(3)	24(1)
O(8)	1706(3)	1656(2)	4763(3)	25(1)
O(9)	385(3)	403(1)	5380(2)	18(1)
O(10)	2028(3)	252(2)	5912(3)	23(1)
O(11)	1577(3)	46(2)	4194(3)	30(1)
O(12)	772(3)	−599(2)	5482(3)	25(1)
O(13)	2954(3)	1711(2)	5583(3)	29(1)
O(14)	4674(3)	1381(2)	5380(3)	27(1)
O(15)	4506(3)	2231(2)	6144(3)	31(1)
O(16)	4056(3)	2176(2)	4282(3)	24(1)
O(17)	2783(3)	1102(2)	4623(3)	25(1)
O(18)	4579(3)	789(2)	4382(3)	32(1)
O(19)	3496(3)	278(2)	5605(3)	25(1)
O(20)	2972(3)	287(2)	3766(3)	32(1)
O(21)	5780(3)	837(2)	5264(3)	29(1)
O(22)	7203(3)	440(2)	4181(3)	28(1)
O(23)	7332(3)	508(2)	6048(3)	31(1)
O(24)	7524(3)	1305(2)	4837(3)	33(1)
O(25)	−1794(3)	3263(2)	4176(3)	37(1)
O(26)	542(3)	2583(2)	7011(3)	22(1)
O(27)	−511(3)	2412(2)	2994(3)	24(1)
O(28)	651(3)	771(2)	4132(3)	27(1)
O(29)	1949(3)	1120(2)	5841(3)	24(1)
O(30)	5575(3)	1378(2)	4207(3)	27(1)
O(31)	6912(3)	−81(2)	3095(3)	27(1)
O(32)	7971(3)	99(2)	7122(3)	25(1)
N(1)	6910(4)	1159(2)	3140(4)	27(2)
N(2)	6640(5)	1521(2)	1765(4)	32(2)
N(3)	8403(5)	1575(3)	3260(4)	40(2)
N(4)	8089(5)	1067(2)	2016(4)	32(2)
N(5)	8089(4)	1999(3)	1837(4)	36(2)
N(6)	7026(4)	2082(2)	2953(4)	29(2)
N(7)	5514(4)	445(3)	6912(4)	34(2)
N(8)	5576(4)	1369(2)	6925(4)	23(2)
N(9)	4098(4)	935(2)	6778(3)	20(2)
N(10)	580(4)	471(2)	6979(3)	20(2)
N(11)	−826(4)	965(2)	6675(3)	20(2)
N(12)	654(4)	1379(2)	6980(3)	20(2)
C(1)	6256(5)	966(3)	2668(5)	29(2)
C(2)	5930(5)	1328(3)	2177(5)	29(2)
C(3)	9061(6)	1289(4)	2971(6)	48(3)
C(4)	8723(7)	917(4)	2555(6)	59(3)
C(5)	7704(5)	2437(3)	1910(5)	30(2)
C(6)	7492(4)	2474(3)	2752(5)	28(2)
C(7)	5108(5)	22(3)	7090(5)	41(3)
C(8)	6223(5)	1550(3)	7437(5)	30(2)
C(9)	3429(5)	1170(3)	7153(5)	31(2)
C(10)	1242(5)	1566(3)	7542(5)	30(2)
C(11)	142(5)	51(3)	7095(4)	26(2)
C(12)	−1534(5)	1196(3)	6981(5)	27(2)

[a] *U*(eq) is defined as one-third of the trace of the orthogonalized U^{ij} tensor.

Table 3. Atomic Coordinates ($\times 10^4$) and Equivalent Isotropic Displacement Parameters ($Å^2 \times 10^3$) for 2

	x	*y*	*z*	*U*(eq)[a]
Zn(1)	400(1)	3333(1)	5441(1)	17(1)
Zn(2)	6667	3333	6494(1)	18(1)
Co(1)	0	0	2500	16(1)
Cl(1)	6667	3333	7500	33(1)
P(1)	3544(2)	3191(2)	5828(1)	15(1)
O(1)	505(5)	5436(5)	5656(2)	28(1)
O(2)	1450(5)	3493(5)	4681(2)	19(1)
O(3)	1677(5)	2709(5)	5966(2)	20(1)
O(4)	4312(5)	2736(5)	6331(2)	23(1)
O(1W)	3333	-3333	6531(11)	235(14)
N(1)	−1778(6)	91(6)	2961(2)	24(1)
C(1)	−2516(8)	1025(9)	2650(3)	31(2)

[a] *U*(eq) is defined as one-third of the trace of the orthogonalized U^{ij} tensor.

mixture including ethanol/water (1:1) instead of water to carry out the synthesis of **1** while keeping the same filling volume of 50%. The final product using the solvent mixture contained both **1** and **2**, as expected. This is because ethanol has a higher vapor pressure than water, thus increasing the pressure of the reaction system. It can be concluded that lower pressure in the reaction system favors the crystallization of **1** and that higher pressure in the reaction system favors the crystallization of **2** for the above gel composition.

As a consequence, decreasing the crystallization temperature, which causes the reaction pressure to decrease, will have an influence on the product. When the above reaction gel is heated at 110−130 °C, no matter what the filling volume is, the product is phase **1**. From later structural discussions, it can be seen that the difference between **1** and **2** is that **1** is a 2D layered compound templated by $Co^{II}(en)_3^{2+}$ cations and that **2** is a 3D compound templated by $Co^{III}(en)_3^{3+}$ cations where μ-Cl atom is involved in the coordination of tetrahedral Zn atoms. The formation of $Co^{II}(en)_3^{2+}$ cations is due to the reduction of the initial $Co^{III}(en)_3Cl_3$ complex under hydrothermal reaction conditions. Our experimental results indicate that variation of the reaction pressure affects the crystallization mechanisms by which **1** is assembled from the $Co^{II}(en)_3^{2+}$ template and **2** is assembled from the $Co^{III}(en)_3^{3+}$ template in the above gel system. Further study on this aspect is underway.

Figures 1 and 2 show the experimental and simulated X-ray diffraction patterns for **1** and **2**, respectively. The experimental XRD patterns for both **1** and **2** are in accord with the simulated XRD patterns generated on the basis of the structural data except for some intensity differences.

ICP analyses for **1** and **2** indicate that **1** contains 25.1, 7.3, and 15.8 wt % of Zn, Co, and P, respectively (calcd 23.9, 7.19, and 15.1 wt %, respectively), and that **2** contains 35.7, 4.04, and 12.8 wt % of Zn, Co, and P, respectively (calcd 37.3, 4.20, and 13.3 wt %, respectively). Elemental analyses indicate that **1** contains 9.1, 3.8, and 11.0 wt % of C, H, and N, respectively (calcd 8.8, 3.45, and 10.3 wt %, respectively), and that **2** contains 5.33, 1.89, and 5.73 wt % of C, H, and N, respectively (calcd 5.13, 2.0 and 6.0 wt %, respectively). The compositional analyses are in agreement with the values calculated using the formulas $[Co^{II}(en)_3]_2[Zn_6P_8O_{32}H_8]$ for **1** and $[Co^{III}(en)_3][Zn_8P_6O_{24}Cl]\cdot 2H_2O$

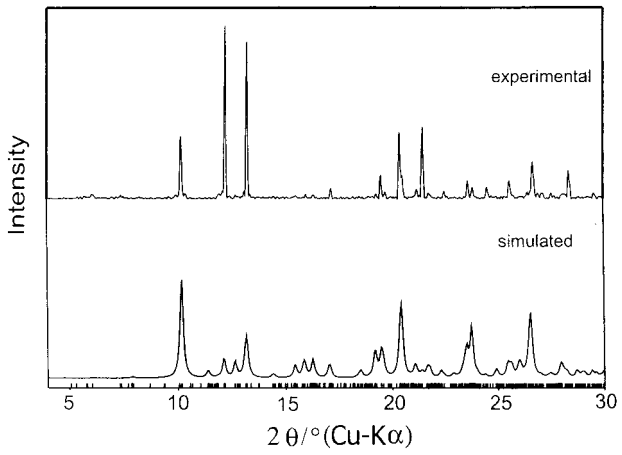

Figure 1. Experimental and simulated X-ray powder diffraction patterns for **1**.

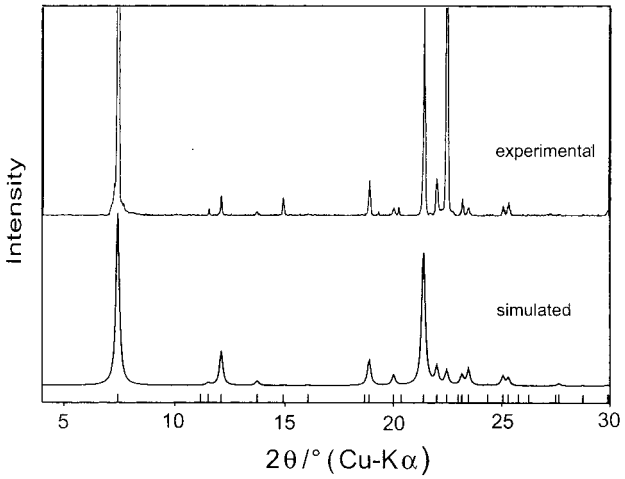

Figure 2. Experimental and simulated X-ray powder diffraction patterns for **2**.

for **2** that were given by single-crystal X-ray diffraction analyses.

The thermal properties of the **1** and **2** were investigated using TG analysis. **1** shows a weight loss of about 22.3 wt % occurring at 300−700 °C, which is attributed to the decomposition of the metal complex (calcd 22%). For **2**, a weight loss of about 3.0 wt % occurs below 200 °C, which is attributed to the loss of the water molecules inside the tunnels. A weight loss of 13.0 wt % at about 370 °C indicates the decomposition of the metal complex (calcd 12.8%). X-ray powder diffraction indicates that, after the decomposition of the metal complex, the structures of **1** and **2** collapse. Upon calcination of samples of **1** and **2** to 800 °C, mixtures of dense phases of $ZnPO_4$ and $CoPO_4$ are formed.

Single-crystal X-ray diffraction analysis indicates that **1** crystallizes in the monoclinic space group *C*2/*c*. The asymmetric unit contains 73 non-hydrogen atoms, as shown in Figure 3, of which 46 atoms belong to the host network and 27 atoms to the guest metal complex species. There are six crystallographically distinct Zn and eight crystallographically distinct P atoms. The zinc atoms are tetrahedrally coordinated by oxygen atoms with Zn−O bond lengths in the range of 1.905(5)−2.005(5) Å. The O−Zn−O angles are in the range of 95.03(10)−123.7(2) Å. The P atoms are also tetrahedrally coordinated by oxygen atoms and share three oxygen atoms with adjacent Zn atoms, with P−O distances in the range of 1.505(5)−1.541(5) Å, leaving one oxygen atom terminus with the longer P−OH distances in the range of 1.544(5)−1.614(5) Å. There are three crystallographically distinct Co atoms in each asymmetric unit. Whereas Co(1) atom lies at a general position, both Co(2) and Co(3) lie at special position on the 2-fold axis and $\bar{1}$-fold axis, respectively. Assuming the usual valences of Zn, P, O, and H to be +2, +5, −2, and +1, respectively, the network stoichiometry of $[Zn_6P_8O_{32}H_8]$ creates a net charge of −4. The presence of two $Co(en)_3$ molecules would account for +4 arising from the Co(II). The existence of Co(II) is due to the reduction of

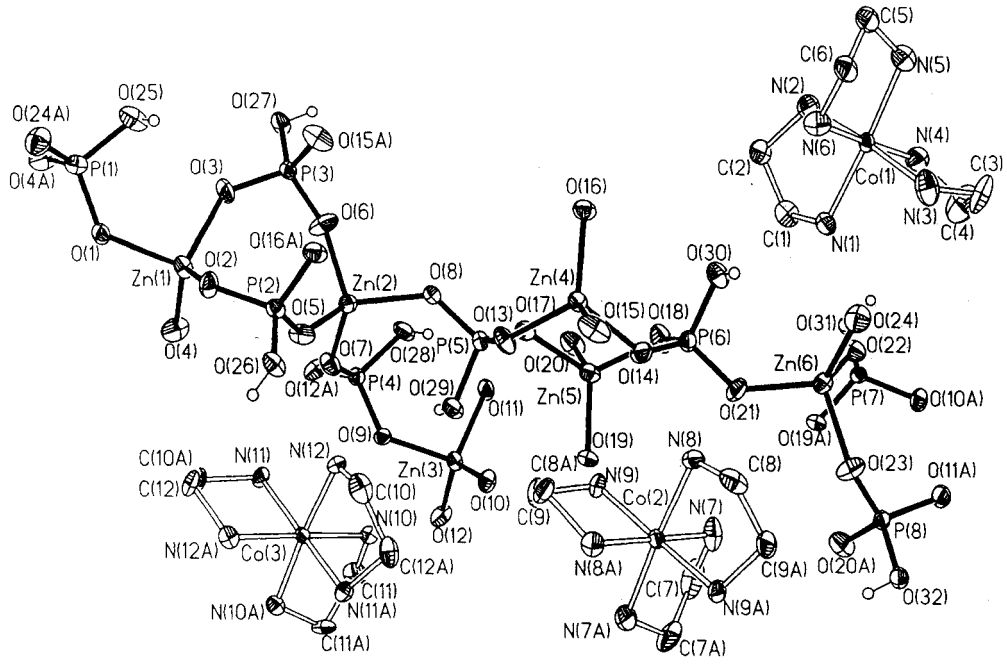

Figure 3. ORTEP plot of **1**, $[Co^{II}(en)_3]_2[Zn_6P_8O_{32}H_8]$. Thermal ellipsoids are given at 50% probability.

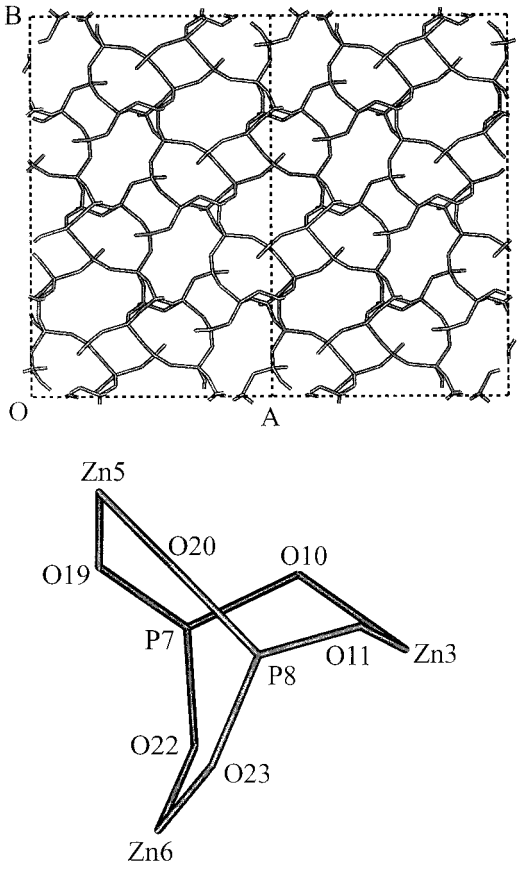

Figure 4. (a) Sheet structure of **1** viewed along the [001] direction and (b) a propellane-like chiral structural motif.

Co(III) in $Co(en)_3Cl_3$ under the hydrothermal reaction conditions.

The structure of **1** is built from strictly alternating ZnO_4 and $PO_3(OH)$ tetrahedra that are linked through their vertexes, giving rise to the two-dimensional layered structure with a 4.6.8 net seen in Figure 4a. Interestingly, the sheet contains a series of chiral structural motifs, which is similar to [3.3.3] propellane, as shown in Figure 4b. The chiral structural motif has also been found in the layered aluminophosphate $[Co(en)_3][Al_3P_4O_{16}]3H_2O$ with 4.6 nets.[8] This motif is chiral as it has a distinct twist in one direction. Even though the overall structural is not chiral, the structure of **1** indicates that the chiral feature of the metal complex can be transferred to the inorganic lattice.

Figure 5 shows the packing of the inorganic sheets along the *c* direction. Interestingly, the enantiomers of the cobalt complexes are separated as Δ and Λ configurations in alternate interlayer regions. The orderly separation of the enantiomers of the metal complex indicates that the inorganic host has a molecular recognition ability for the guest metal complex. There are extensive hydrogen-bonding interactions between the amino groups of the cobalt complex and the lattice oxygen atoms, with the N···O distances in the range of 2.813(7)−3.084(8) Å. Table 4 lists a summary of the H-bonding information. H-bonding interactions also exist between the P−OH groups protruding into the interlayer region. Each such OH group serves as both a H-bond donor and a H-bond acceptor to another OH group in an adjacent layer.

Single-crystal X-ray diffraction analysis indicates that **2** crystallizes in the trigonal space group $P\bar{3}1c$ (no. 163). The asymmetric unit contains 12 non-hydrogen atoms, as shown in Figure 6, with two Zn and one P atoms being crystallographically distinct. The tetrahedral P

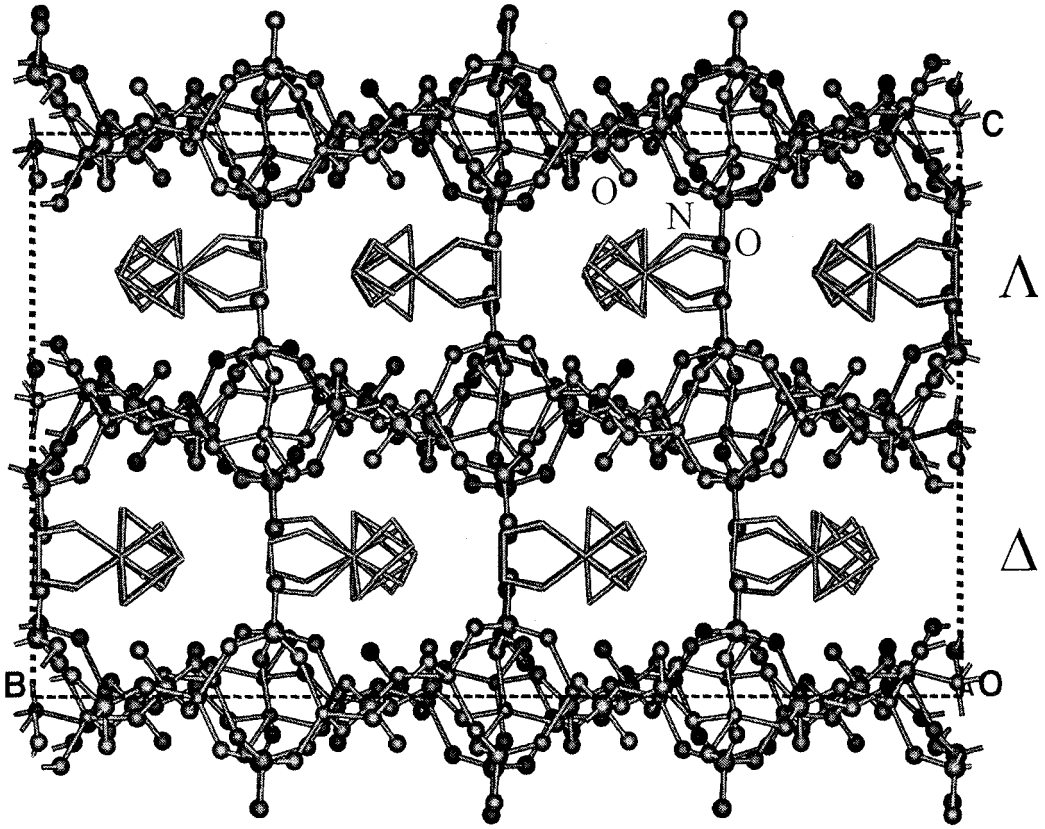

Figure 5. Packing of the inorganic layers along the [001] direction with the cobalt complexes residing in the interlayer region. Δ and Λ stand for the absolute configurations of chiral $Co(en)_3^{2+}$ cations.

Table 4. Summary of H-Bonding between the Host Lattice and Guest Metal Complexes

D−H···A[a]	d(D···A) (Å)	∠(DHA) (°)
N(1)−H(1A)···O(22)	2.893(8)	137.8
N(1)−H(1B)···O(30)	2.980(8)	142.3
N(2)−H(2A)···O(16)#7	2.944(9)	149.9
N(2)−H(2B)···O(17)#7	2.908(8)	165.1
N(4)−H(4B)···O(28)#7	3.043(8)	127.4
N(5)−H(5B)···O(8)#7	3.002(8)	166.6
N(6)−H(6B)···O(1)#4	2.830(8)	167.2
N(8)−H(8A)···O(25)#4	3.019(8)	115.3
N(9)−H(9A)···O(14)	2.957(8)	175.3
N(9)−H(9B)···O(19)	3.034(8)	139.7
N(10)−H(10A)···O(9)	2.813(7)	152.6
N(10)−H(10B)···O(32)#1	3.084(8)	151.3
N(11)−H(11A)···O(7)	3.012(7)	156.6
N(12)−H(12A)···O(29)	3.045(7)	156.5
N(12)−H(12B)···O(5)	2.895(8)	139.7

[a] Symmetry transformations used to generate equivalent atoms: #1 $-x+1, y, -z+3/2$; #4 $-x+1/2, -y+1/2, -z+1$; #7 $-x+1, y, -z+1/2$.

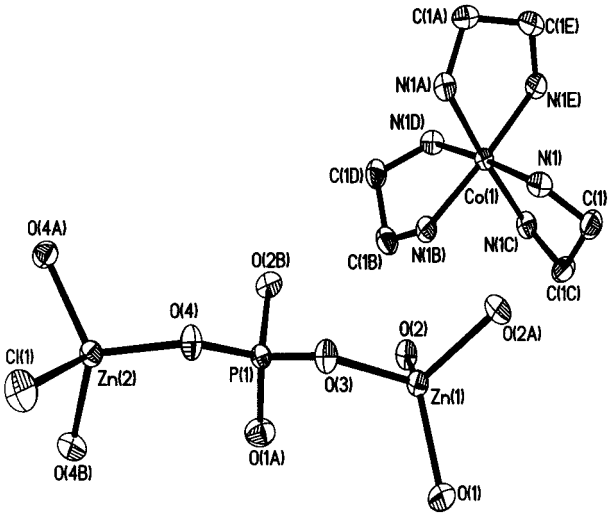

Figure 6. ORTEP plot of **2**, $[Co^{III}(en)_3][Zn_8P_6O_{24}Cl]\cdot 2H_2O$. Thermal ellipsoids are given at 50% probability.

atom shares four oxygen atoms with adjacent Zn atoms, with P−O bond lengths in the range of 1.502−1.567(4) Å. Zn(1) shares four oxygen atoms with adjacent P atoms, with Zn−O bond lengths in the range of 1.893−2.004 (4) Å. A μ_3-O(2) exists, which bridges two Zn(1) atoms and one P atoms. Zn(2) atom shares three oxygens with adjacent P atoms, with Zn−O bond lengths of 1.922(4) Å and with the fourth ligand being a μ-Cl atom located in the 32-fold axis (Wyckoff notation *d*), which bridges two Zn(2) atoms via a Zn−Cl−Zn linkage. The Zn(2)−Cl bond length is 2.392(1) Å, which is typical for Zn−Cl covalent bond distances.[25] The Zn−Cl−Zn bond angle is 180°. To our knowledge, this is the first framework material involving bridging chlorine as a framework element in the manner of a bridging oxygen atom. Recently, in the layered zinc chlorophosphate $[C_6NH_{14}][ZnCl(HPO_4)]$,[26] a terminal Zn−Cl bond of 2.220 Å was found wherein the Cl^- ion is part of the network. Each asymmetric unit also contains one crystallographically distinct Co atom located on a site of 32-fold

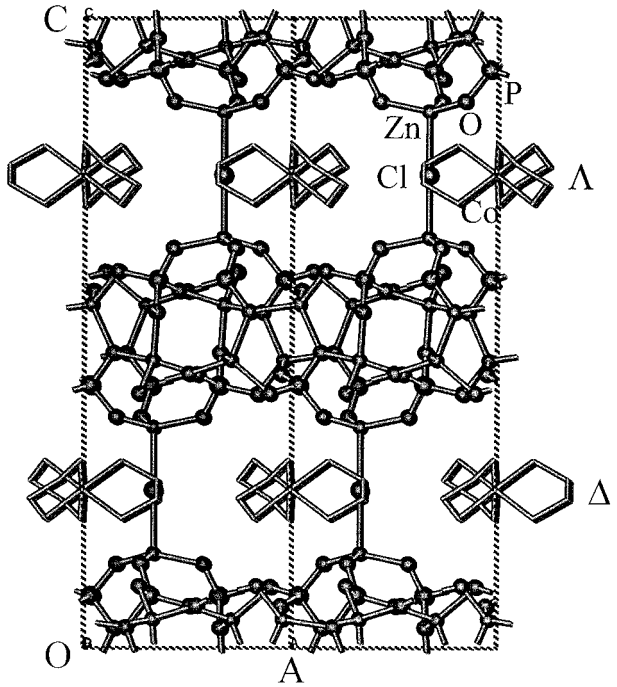

Figure 7. Framework structure of **2** viewed along the [010] direction. Δ and λ stand for the absolute configurations of chiral $Co(en)_3^{3+}$ cations. Water molecules inside the tunnels are not shown.

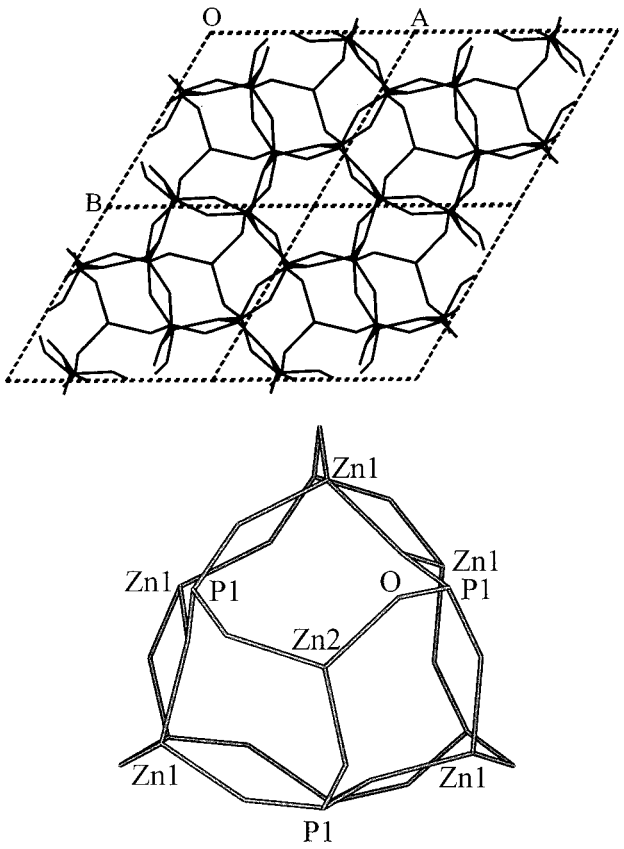

Figure 8. (a) Zinc phosphate layer in **2** viewed along the [001] direction and (b) a caplike chiral structural motif.

symmetry. The stoichiometry of $[Zn_8P_6O_{24}Cl]$ would result in a net framework charge of −3. The presence of one molecule of $Co(en)_3$ would account for a +3 charge arising from the Co(III). Unlike **1**, the valence state of Co(III) in **2** does not change from that in the initial Co-

(25) (a) Brynestad, J.; Yakel, H. L. *Inorg. Chem.* **1978**, *17*, 1376. (b) Selenium, C. O.; Delaplane, R. G. *Acta Crystallogr. B.* **1978**, *34*, 1330. (c) Forsberg, H. E.; Nowachi, W. *Acta Chemica Scandinavica* **1959**, *13*, 1049.

(26) Neeraj, S.; Natarajan, S. *J. Mater. Chem.* **2000**, *10*, 1171.

Table 5. Summary of H-Bonding Informations for 2 between the Host Lattice and Metal Complexes

D−H···A[a]	*d*(D···A)	∠(DHA)
N(1)−H(1)···O(4)#13	2.922(6)	146.9
N(1)−H(2)···O(3)#1	2.827(6)	161.8

[a] Symmetry transformations used to generate equivalent atoms: #1 $x - y$, x, $-z + 1$; #13 $-x$, $-y$, $-z + 1$.

$(en)_3Cl_3$ complex under hydrothermal conditions.

The ZnO_4, ZnO_3Cl, and PO_4 tetrahedra are linked via vertex oxygen atoms and bridging Cl atoms to form a three-dimensional connected framework containing intersecting 12-MR tunnels (Cl···Cl distance = 8.9 Å), as shown in Figure 7. The framework structure of **2** can alternatively be viewed as the stacking of the zinc phosphate layers along the *c* axis with Cl atoms as pillars. As depicted in Figure 8a, the thick zinc phosphate layer is built up from alternating PO_4 units and $Zn(1)O_4$ and $Zn(2)O_3$ units forming a 2D porous network parallel to the *ab* plane. Interestingly, the sheet structure of **2** contains a series of novel caplike chiral motifs composed of six 4-MRs and three 3-MRs, with the top of the cap being a Zn(2) atom, as shown in Figure 8b. Clearly, the chirality of this chiral structural motif is transferred from the chiral $Co(en)_3Cl_3$ complex.

Cobalt complexes reside in the tunnels enclosed by adjacent layers and Cl atoms. Interestingly, as with compound **1**, the enantiomers of the cobalt complex are separated in an orderly fashion as Δ and Λ configurations in alternate zinc phosphate layers and interact with the host through extensive H-bonding interactions. Each amino group of the cobalt complex forms two H-bonds to bridging oxygens in the layers, with N···O separations of 2.827(6) and 2.922(6) Å. Table 5 lists a summary of the H-bonding information for **2**.

Insight into the structures of **1** and **2** clearly provides evidence that the chiral metal complex can induce its chiral feature in an inorganic lattice. On the other hand, the orderly separation of the enantiomers of the cobalt complex into Δ and Λ configurations indicates that there exists molecular recognition ability between the host inorganic and the guest metal complex. The H-bonding interactions between the chiral metal complex and the host lattice might account for the chiral transference and molecular recognition. Further investigation of the mechanism by which the inorganic host assembles about the chiral metal complex will be of significant importance.

Conclusions

Hydrothermal synthesis of the two new zinc phosphates $[Co^{II}(en)_3]_2[Zn_6P_8O_{32}H_8]$ (**1**) and $[Co^{III}(en)_3][Zn_8P_6O_{24}Cl]\cdot 2H_2O$ (**2**) has been accomplished in the same reaction gel system using a racemic mixture of a chiral metal complex as the template. Variations in the reaction pressure have a critical influence on the crystallization of these two phases. Both structures **1** and **2** contain chiral structural motifs, the chiral characters of which are believed to be transferred from the chiral metal complex. The enantiomers of $Co(en)_3Cl_3$ are separated as Δ and Λ configurations in an orderly fashion in the structures of both **1** and **2** and interact with the inorganic host through extensive H-bonding interactions. Further studies on the mechanism by which the host lattice is assembled by the chiral metal complex will assist in the rational design of nanoporous chiral materials.

Acknowledgment. This work is supported by the National Natural Science Foundation of China and the State Basic Research Project of China (G2000077507). J.Y. acknowledges the support of the Teaching and Research Award Program for Outstanding Young Teachers in Higher Education Institutions of MOE, P.R.C.

Supporting Information Available: Crystallographic data for **1** and **2** (PDF/CIF). This material is available free of charge via the Internet at http://pubs.acs.org.

CM010302F